A graphical approach to determine the relationship between intercept, gradient, and the common seismic rock properties: Global model and application

David Went[1]

https://doi.org/10.1190/tle44030224.1

Abstract

Globally applicable forward amplitude variation with offset models of sand-shale systems are displayed using the intercept-gradient crossplot, color coded by the magnitude of reflectivity of the common seismic rock properties: bulk modulus, shear modulus, Lamé's parameter lambda, Poisson's ratio, and V_P/V_S. Lines of equal magnitude are threaded through the data to establish the angular relationship of each rock property to intercept and gradient. In many cases, these generic models will be sufficient to design a seismic inversion capable of distinguishing lithology and fluid. An inverted seismic section over a producing field illustrates how fluid-sensitive (rEEIχ27) and fluid-insensitive (shear-impedance) attributes conform closely to the generic model. Where suitable data exist, the modeling process can be modified to provide a more tailored reservoir characterization and inversion routine.

Introduction

Analysis of amplitude variation with offset (AVO) or amplitude variation with angle (AVA) is an integral part of the prospecting process in many plays globally. It is also key in reservoir characterization as part of field development and for monitoring production. It typically involves measurement of the amplitude at zero offset (termed the intercept [I]) and the rate at which amplitude changes with incidence angle (termed the gradient [G]), using either seismic gathers or angle stacks. The most common reason for doing it is to determine fluid type (hydrocarbon versus brine) and to discriminate the effects of fluid, lithology, and porosity. Certain rock properties are commonly noted to be key to establishing these effects. For example, the shear modulus (μ), by definition in Gassmann's law (Gassmann, 1951; Smith et al., 2003), is insensitive to fluid type. Shear impedance is closely related to shear modulus and also displays a very low sensitivity to fluid type. On the other hand, acoustic impedance, bulk modulus, Lamé's parameter lambda (λ), Poisson's ratio (σ), and V_P/V_S are far more sensitive to fluid changes. The equivalence of the common seismic rock properties to elastic or extended elastic impedance at different angles has been made previously, though typically more as an aside than as a focus of study (e.g., Mallick, 2001; Whitcombe et al., 2002). The purpose of this paper is to describe a simple graphical method to establish the relationship between the common rock properties and intercept and gradient, and to show how they can be generated from seismic data. The method can be used to generate other rock properties (e.g., Young's modulus) or to provide a more bespoke reservoir characterization, where suitable log data are available.

Rock properties and angle-dependent seismic reflectivity

Most geoscientists working in the subsurface with seismic data will be aware that contrasts in impedance are the cause of seismic reflections. When building a normal incidence synthetic seismogram, the sonic and density logs are used to calculate acoustic impedance. Changes in acoustic impedance at reflecting interfaces result in either a positive or negative reflection coefficient (spikes), the magnitude of which is defined by equation 1:

$$I2 - I1/(I1 + I2), \quad (1)$$

where $I1$ is the impedance of the incident rock, and $I2$ is the impedance of the reflecting rock.

When a reflection coefficient series is convolved with a wavelet, it yields a synthetic seismic trace. The earlier acoustic-impedance-generated seismogram is only strictly valid at zero offset. With increasing incidence angle, contrasting lithologies shear at different rates, which necessitates contrasts in shear velocity to be added into the equation. Hence, reflectivity becomes defined by contrasts in elastic (angle-dependent) impedance rather than acoustic impedance (Mukerji et al., 1998; Connolly, 1999; Whitcombe et al., 2002). The rate at which P-wave reflection coefficient changes with offset is described by the Zoeppritz equation, or more practically, one of the approximations to it (most commonly the Shuey equation) (Zoeppritz, 1919; Shuey, 1985). To build a forward model of angle-dependent reflectivity, V_P, V_S, and density are required for the incident and reflecting rocks. Generic global models of angle-dependent reflectivity for sandstones and shales using the Shuey equation were presented by Went (2021). These models illustrate a full range of possible outcomes for intercept and gradient based on geologically feasible combinations of V_P, V_S, and density. Models are depth dependent and may be corroborated by other global studies (e.g., Mur and Vernik, 2019).

Method

The most common rock properties, their common abbreviations, and formulae (different combinations of V_P, V_S, and density) are listed in Table 1. The V_P, V_S, and density data used by Went (2021) to generate globally applicable intercept and gradient results

Manuscript submitted 6 August 2024; accepted 3 October 2024.
[1]TGS Geophysical ASA, Weybridge, UK. E-mail: david.went@tgs.com.

for a depth of 1750 m below sea bed in a normally compacting basin are shown in Table 2. The resulting model is displayed in Figure 1. The same data are used to generate the common seismic rock properties, acoustic impedance, shear impedance, bulk modulus, Lamé's parameter lambda, shear modulus, Poisson's ratio, and V_P/V_S. These are also displayed in Table 2. Because the common rock properties are each described by different combinations of V_P, V_S, and density, they are, in essence, different forms of elastic impedance. The reflection coefficient for each of the main rock properties (e.g., shear modulus for shale 1 over sand 1) can be calculated using equation 1, in the same way as for any other impedance contrast. The results for each of the seismic rock properties in each of the cases (shale 1 over sand 1, shale 1 over sand 2, etc.) are shown in the lower part of Table 2. Gassmann fluid substitution was used to generate modified V_P, V_S, and density values (not shown) in the presence of hydrocarbons, using the following in-situ fluid properties: oil density (0.7), bulk modulus (0.85), water density (0.98), and bulk modulus (2.57). These modified values are used to generate each hydrocarbon case reflection coefficient.

The reflection coefficient data for each seismic rock property were sorted by magnitude. The intercept-gradient crossplot data were then color coded by the magnitude of each seismic rock property to enable the angular relationships to be visualized, determined, and compared.

Table 1. Seismic rock properties, their common abbreviations, and equations used to generate them from well logs and seismic data.

Attribute	Abbreviation	Equation
Velocity	V_P	V_P
Shear velocity	V_S	V_S
Density	ρ	ρ
Acoustic impedance	AI	ρV_P
Shear impedance	SI	ρV_S
Bulk modulus	K	$\rho V_P^2 - 4/3\mu$
Shear modulus	μ	ρV_S^2
Lamé's lambda	λ	$\rho V_P^2 - 2\mu$
Poisson's ratio	σ	$V_P^2 - 2V_S^2/2(V_P^2 - V_S^2)$
V_P/V_S	V_P/V_S	V_P/V_S

Results

Displays of crossplots of intercept versus gradient, color coded by the reflectivity of the evaluated seismic rock properties, are shown in Figures 2 and 3. Each intercept-gradient crossplot is shown twice: (1) with a clear view of the data color coded for the attribute and (2)

Table 2. Global model data for 1750 m TVDBSB (after Went, 2021). Rock properties are calculated from the model data. Rock property reflectivity is prefixed R_ and is for shale 1 over shale 2, sand 1, sand 2, sand 3, and sand 4. HC denote a hydrocarbon case.

Input data	Shale 0	Shale 1	Shale 2	Org. Sh	Sand 1	Sand 2	Sand 3	Sand 4
V_P (km/s)	2.700	3.048	3.260	2.700	3.672	3.300	3.048	2.800
V_S (km/s)	1.212	1.480	1.643	1.420	2.097	1.798	1.595	1.396
Density (g/cc)	2.27	2.35	2.40	2.22	2.32	2.25	2.20	2.16
AI (GPa)	6.14	7.17	7.81	5.99	8.51	7.43	6.72	6.04
SI (GPa)	2.76	3.48	3.94	3.15	4.86	4.05	3.52	3.01
V_P/V_S	2.23	2.06	1.98	1.90	1.75	1.84	1.91	2.01
Poisson's ratio σ	0.37	0.35	0.33	0.31	0.26	0.29	0.31	0.33
Bulk modulus K (GPa)	12.13	14.99	16.85	10.22	17.66	14.81	13.00	11.30
Lambda λ (GPa)	9.90	11.56	12.53	7.23	10.87	9.96	9.26	8.50
Shear modulus μ (GPa)	3.34	5.15	6.47	4.48	10.20	7.28	5.61	4.20
Porosity ø (%)					20%	24%	27%	30%
R_V_P/V_S		−0.039	−0.019	−0.040	−0.081	−0.058	−0.038	−0.013
R_V_P/V_S HC					−0.105	−0.093	−0.081	−0.067
R_σ		−0.039	−0.024	−0.057	−0.146	−0.090	−0.053	−0.017
R_σ HC					−0.227	−0.178	−0.144	−0.114
R_SI		0.116	0.062	−0.049	0.166	0.075	0.005	−0.073
R_SI HC					0.163	0.071	−0.002	−0.080
R_μ		0.213	0.113	−0.070	0.329	0.171	0.043	−0.101
R_K		0.105	0.058	−0.189	0.082	−0.074	−0.071	−0.140
R_KHC					−0.009	−0.124	−0.212	−0.306
R_Lambda		0.077	0.041	−0.230	−0.031	−0.074	−0.110	−0.152
R_Lambda HC					−0.187	−0.258	−0.316	−0.383

with dashed "contour" lines separating seismic rock properties of different magnitudes. These straight lines are threaded between the data points and clearly illustrate the angle of rotation (chi [χ]) on the intercept-gradient crossplot the seismic rock property represents.

A color-coded display of acoustic-impedance reflectivity is not really needed because it is the same as intercept reflectivity. In other words, the color coding would reveal vertical lines of equal magnitude, confirming acoustic impedance is the same as

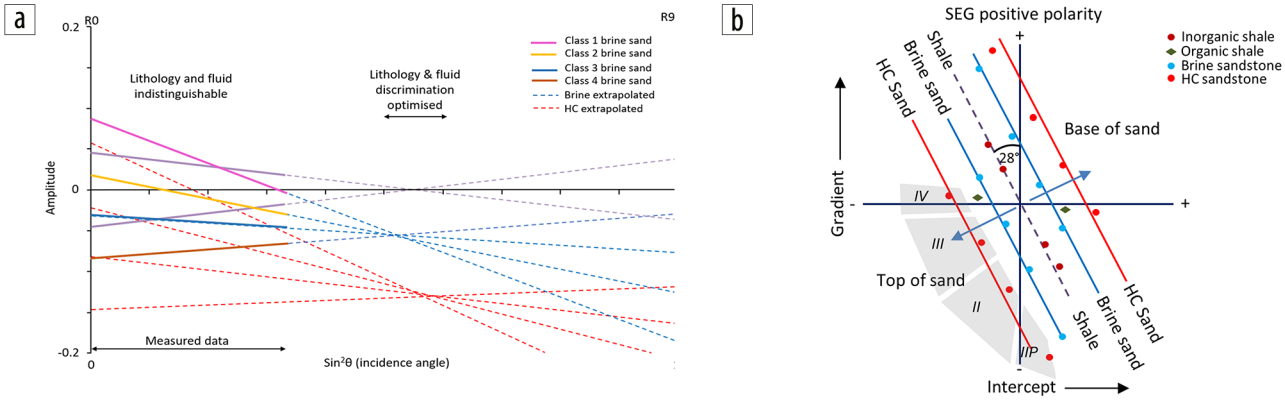

Figure 1. (a) Angle-dependent reflectivity plot of $\sin^2\theta$ versus amplitude or reflection coefficient showing intercept and gradient for the cases in Table 2 extrapolated to 90°. (b) The same data plotted as an intercept versus gradient crossplot color coded for shale over rock type. Global model for 1750 m TVDBSB (after Went, 2021).

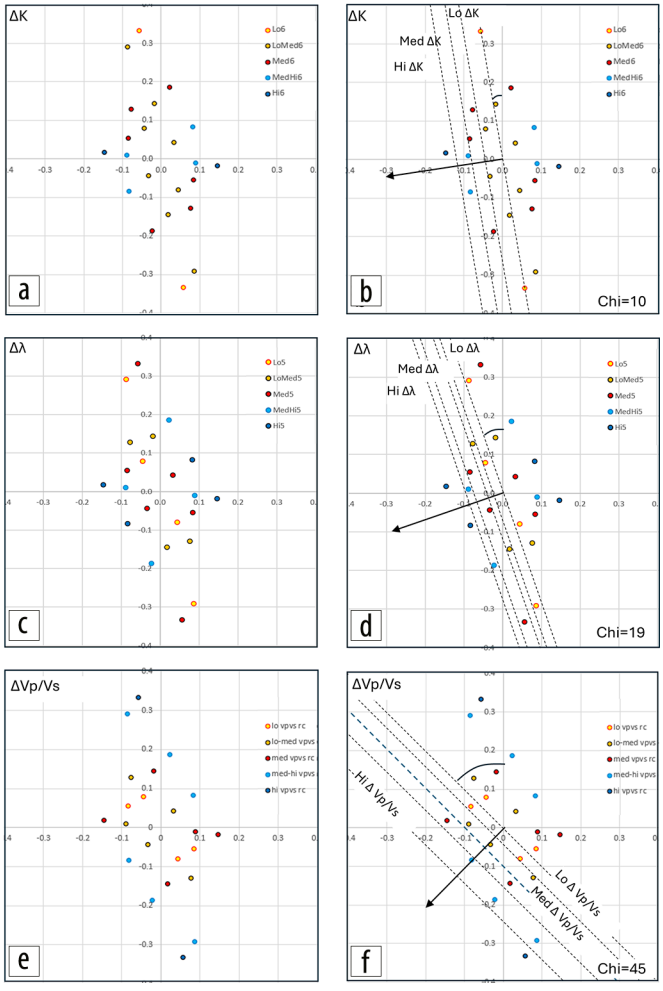

Figure 2. Intercept-gradient crossplots color coded by moduli reflectivity: (a) and (b) bulk modulus, (c) and (d) λ, and (e) and (f) V_p/V_s. Plots (b), (d), and (f) show dashed lines separating moduli reflectivity of different magnitude. The lines define the χ angle.

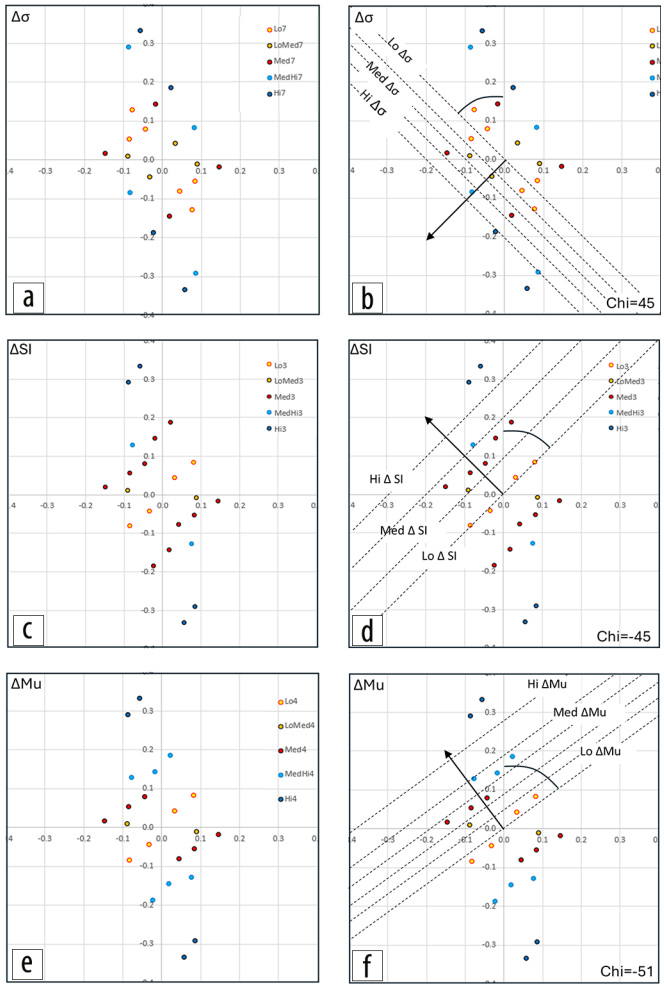

Figure 3. Intercept-gradient crossplots color coded by moduli reflectivity: (a) and (b) Poisson's ratio (σ), (c) and (d) shear impedance, and (e) and (f) shear modulus (μ). Plots (b), (d), and (f) show dashed lines separating moduli reflectivity of different magnitude. The lines define the χ angle.

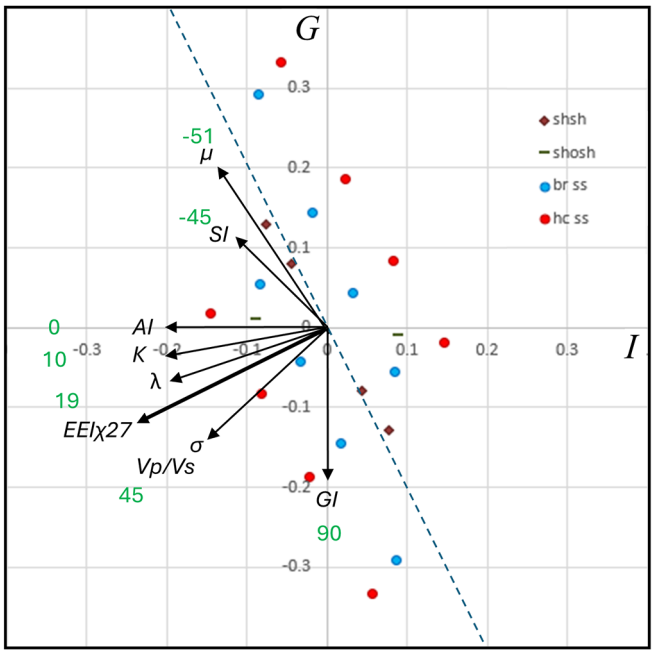

Figure 4. Intercept-gradient crossplot color coded by lithology and fluid, showing the relationship to the common rock property vectors as defined by the graphical determination. Global model for 1750 m TVDBSB.

intercept reflectivity, with an increasingly negative reflection coefficient displayed to the left on the x-axis of the crossplot.

The color-coded display of bulk modulus reflectivity allows the threading of lines of equal reflection coefficient that are inclined at a crossplot rotation angle (χ) of 10° from the vertical (Figures 2a and 2b). A similar plot but with lines of equal reflection coefficient defining a rotation angle of 19° defines Lamé's parameter lambda (Figures 2c and 2d).

The color-coded display of V_P/V_S reflectivity shows lines of equal reflectivity substantially rotated, defining a crossplot rotation angle of 45° (Figures 2e and 2f). That is, it has equal parts of intercept and gradient defining it. Poisson's ratio reflectivity is also defined by lines of equal reflectivity, defining a rotation angle of 45° (Figures 3a and 3b). This is not surprising because Poisson's ratio is a monotonic function of V_P/V_S (Table 1).

The color-coded display of shear-impedance reflectivity shows lines of equal reflectivity that run orthogonal to Poisson's ratio reflectivity, defining an attribute oriented at a crossplot (χ) rotation angle of –45° (Figures 3c and 3d). A closely related attribute, shear modulus, shows color-coded data that define a rotation angle (χ) of –51° (Figures 3e and 3f).

The results for all the evaluated rock properties are summarized in Figure 4. The extended elastic impedance attribute EEIχ27 is also displayed as the attribute oriented at the optimal angle to isolate fluid effects. Lambda, Poisson's ratio, and V_P/V_S are oriented, broadly speaking, in a similar direction and are therefore also sensitive to fluid effects. Shear impedance and shear modulus by contrast are oriented in a near orthogonal direction to the fluid-sensitive attributes and should therefore not show a fluid effect in models or seismic inversions.

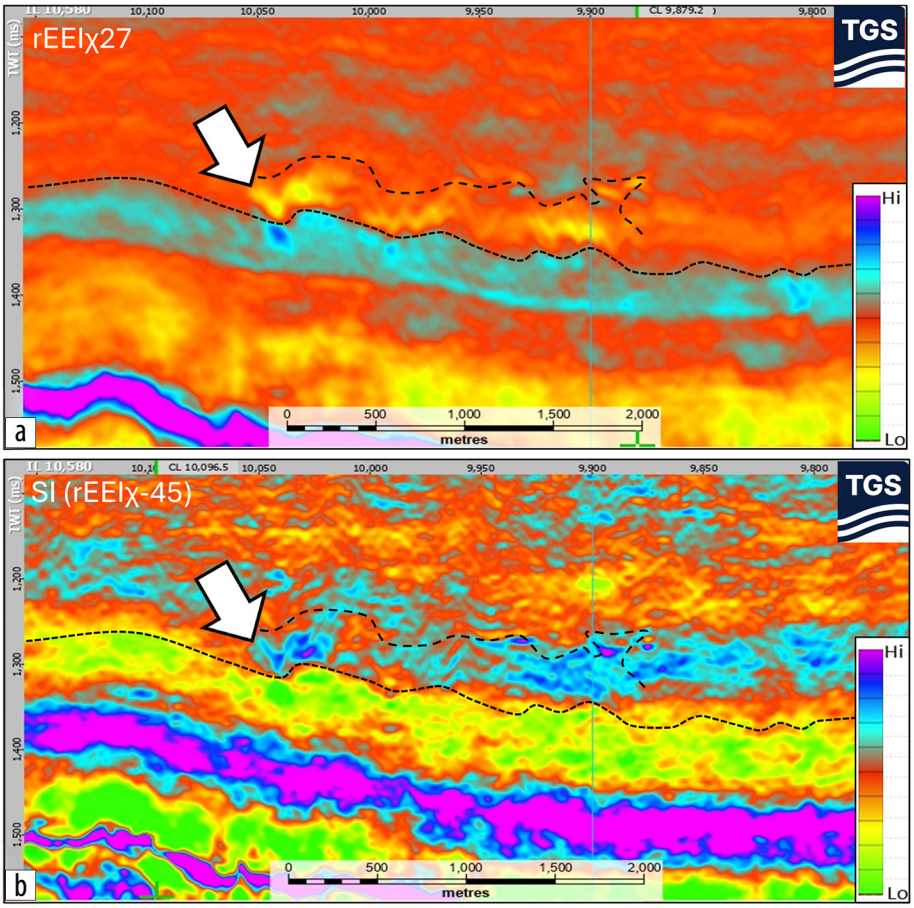

Figure 5. Seismic inversions for (a) rEEIχ27 showing the fluid effect of oil present in a producing North Sea field and (b) shear impedance (rEEIχ–45) where no anomaly is present because shear impedance is insensitive to fluid type. The upper dashed black line (arrowed) marks the top of the oil sands in the producing field, and the lower black dotted line marks the base.

Application

Although the results summarized in Figure 4 were, strictly speaking, determined for a burial depth of 1750 m, they are practically valid over a greater depth range because typical background intercept and gradient relationships change slowly from 1 to 3.5 km of burial (Went, 2021). Figure 5 shows example seismic inversions to test for fluid effects over a proven producing oil field in the North Sea at a depth of 1300 m. The AVO inversions are displayed as relative impedances and were generated following the method described in Went et al. (2023). The rEEIχ27 attribute (Figure 5a) shows a fluid anomaly with low values of rEEIχ27 corresponding to the proven oil in the producing field (hydrocarbon effect). The shear-impedance (rEEIχ-45) attribute (Figure 5b), on the other hand,

shows no such anomaly, consistent with a rock property insensitive to fluid effects and supporting the notion the rEEIχ27 anomaly is indeed a fluid effect caused by an impedance-softening hydrocarbon fluid. Seismic data crossplots of relative acoustic impedance versus gradient impedance, color coded by rEEIχ27 (fluid-sensitive impedance) and rEEIχ-45 (shear impedance), further confirm this conclusion (Figure 6) and conform favorably with the crossplots of the model data (Figures 1b, 2, and 3). Additional field examples demonstrating the applicability of this method are presented in Went et al. (2025).

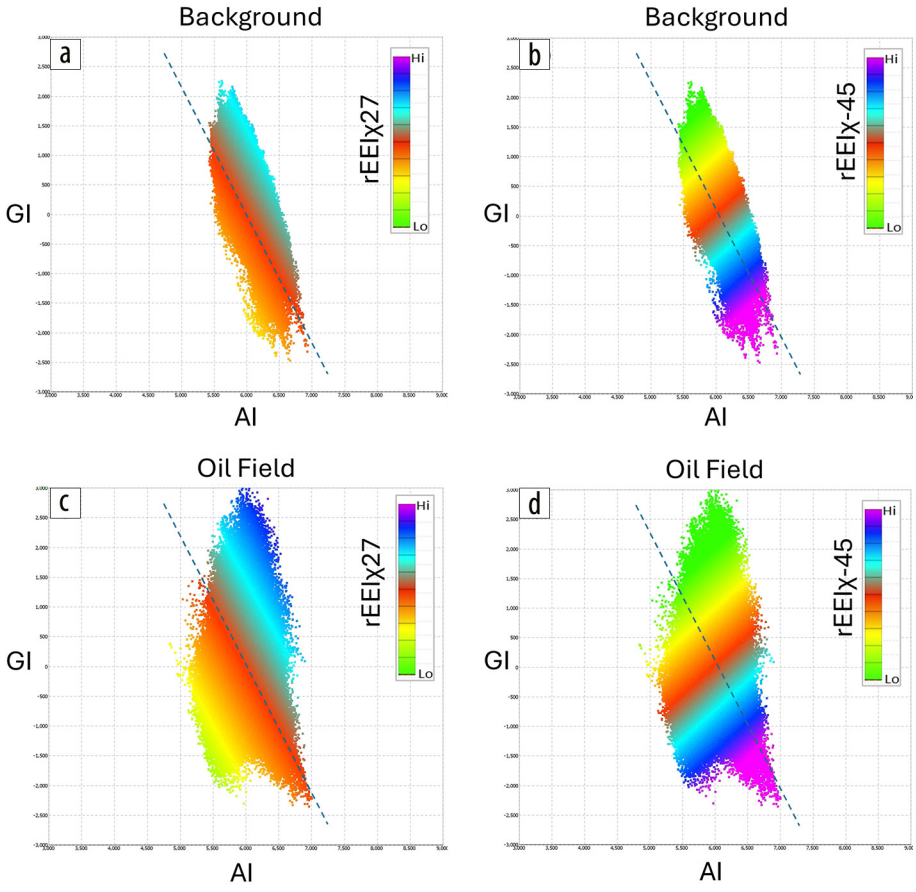

Figure 6. Seismic data crossplots of relative acoustic impedance versus gradient impedance: (a) background location color coded by rEEIχ27 (fluid-sensitive impedance), (b) background location color coded by rEEIχ–45 (shear impedance), (c) producing oil field color coded by rEEIχ27 (fluid-sensitive impedance), and (d) producing oil field color coded by rEEIχ–45 (shear impedance). The oil sands are represented by data in the southwest corner of plots (c) and (d) and are highlighted by anomalously low values (yellow-green) of rEEIχ27 but nonanomalous mid- to high-range values (red-blue) of rEEIχ–45 (shear impedance). Cubes of seismic data are approximately 6 km^2 × 150 m/s.

Conclusion

The common seismic rock properties are each forms of angle-dependent elastic impedance. Reflectivity resulting from contrasts in the common rock properties can be calculated in the same way as for any other impedance contrast. Using previously justified globally applicable model data, the angular relationships of the common rock properties to intercept and gradient are established and displayed. The rock properties broadly group into two classes: (1) those that are fluid sensitive (acoustic impedance, bulk modulus, lambda, Poisson's ratio, and V_P/V_S) and (2) those that are insensitive to fluid effects (shear modulus and shear impedance). Designs for appropriate elastic inversions of seismic data can use the global model presented earlier where log data are either absent or compliant with the model. Alternatively, the modeling process can be performed using local log data to provide a more tailored reservoir characterization and inversion routine. TLE

Acknowledgments

Thanks are due to the two anonymous reviewers for their thoughtful comments and to TGS for permission to publish.

Data and materials availability

Data associated with this research are available and can be obtained by contacting the corresponding author.

Corresponding author: david.went@tgs.com

References

Connolly, P., 1999, Elastic impedance: The Leading Edge, **18**, no. 4, 438–452, https://doi.org/10.1190/1.1438307.

Gassmann, F., 1951, Über die elastizität poröser medien: Vierteljahrsschrift der Naturforschenden Gesellschaft in Zürich, **96**, 1–23.

Mallick, S., 2001, AVO and elastic impedance: The Leading Edge, **20**, no. 10, 1094–1104, https://doi.org/10.1190/1.1487239.

Mukerji, T., A. Jørstad, G. Mavko, and J. R. Granli, 1998, Near and far offset impedances: Seismic attributes for identifying lithofacies and pore fluids: Geophysical Research Letters, **25**, no. 24, 4557–4560, https://doi.org/10.1029/1998GL900187.

Mur, A., and L. Vernik, 2019, Testing popular rock-physics models: The Leading Edge, **38**, no. 5, 350–357, https://doi.org/10.1190/tle38050350.1.

Shuey, R. T., 1985, A simplification of the Zoeppritz equations: Geophysics, **50**, no. 4, 609–614, https://doi.org/10.1190/1.1441936.

Smith, T. M., C. H. Sondergeld, and C. S. Rai, 2003, Gassmann fluid substitutions: A tutorial: Geophysics, **68**, no. 2, 430–440, https://doi.org/10.1190/1.1567211.

Went, D., 2021, Practical application of global siliciclastic rock-property trends to AVA interpretation in frontier basins: The Leading Edge, **40**, no. 6, 454–459, https://doi.org/10.1190/tle40060454.1.

Went, D., M. Bamford, J. Rogers, S. Brown, and G. Turner, 2025, Characterising hydrocarbon discoveries and prospects in the Tay Sandstone using relative elastic inversion: Greater Pilot area, Central North Sea: Proceedings of the First Energy Geoscience Conference, Geological Society, London.

Went, D., R. Hedley, and J. Rogers, 2023, Screening for AVA anomalies in siliciclastic basins: Testing a seismic inversion method in the Mississippi Canyon, Gulf of Mexico: First Break, **41**, no. 9, 75–81, https://doi.org/10.3997/1365-2397.fb2023076.
Whitcombe, D. N., P. A. Connolly, R. L. Reagan, and T. C. Redshaw, 2002, Extended elastic impedance for fluid and lithology prediction: Geophysics, **67**, no. 1, 63–67, https://doi.org/10.1190/1.1451337.
Zoeppritz, K., 1919, Erdbebenwellen VII, VII b, Über Reflexion und Durchgang seismischer Wellen durch Unstetigkeitsflächen: Nachrichten von der Königlichen Gesellschaft der Wissenschaften zu Göttingen.

DOI:10.1190/tle44030224.1